

Redox-Gated Three-Terminal Organic Memory Devices: Effect of Composition and Environment on Performance

Bikas C. Das,^{†,‡,||} Rajesh G. Pillai,^{†,‡,||} Yiliang Wu,[§] and Richard L. McCreery^{*,†,‡}

[†]Department of Chemistry, University of Alberta, Edmonton, Alberta T6G 2M7, Canada

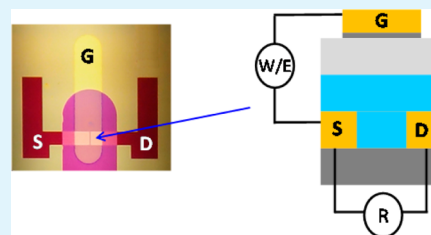
[‡]National Institute for Nanotechnology, National Research Council Canada, Edmonton, Alberta T6G 2M9, Canada

[§]Xerox Research Centre of Canada, 2660 Speakman Drive, Mississauga, Ontario L5K 2L1, Canada

S Supporting Information

ABSTRACT: The performance of redox-gated organic nonvolatile memory (NVM) based on conducting polymers was investigated by altering the polymer structure, composition, and local environment of three-terminal devices with a field-effect transistor (FET) geometry. The memory function was dependent on the presence of a redox active polymer with high conducting and low conducting states, the presence of a redox counter-reaction, and the ability to transport ions between the polymer and electrolyte phases. Simultaneous monitoring of both the “write” current and “readout” current revealed the switching dynamics of the devices and their dependence on the local atmosphere. Much faster and more durable response was observed in acetonitrile vapor than in a vacuum, indicating the importance of polar molecules for both ion motion and promotion of electrochemical reactions. The major factor determining “write” and “erase” speeds of redox-gated polymer memory devices was determined to be the rate of ion transport through the electrolyte layer to provide charge compensation for the conducting polarons in the active polymer layer. The results both confirm the mechanism of redox-gated memory action and identify the requirements of the conducting polymer, redox counter reaction, and electrolyte for practical applications as alternative solid-state nonvolatile memory devices.

KEYWORDS: alternative nonvolatile memory, solid-state redox reactions, conductance switching, resistive memory, multistate memory



INTRODUCTION

The rapid rise of portable consumer electronics has stimulated development of solid-state nonvolatile memory (NVM) devices, with the currently dominant technology being “flash” memory based on the silicon “floating gate” design. The field effect transistor (FET) geometry of flash memory permits high density, while the floating gate yields long retention time, typically >10 years. However, flash memory requires relatively high energy for write and erase operations, and the cycle life is limited compared to disk drives and dynamic random access memory (DRAM). A large number of alternative NVM (ANVM) devices including metal/insulator/metal crossbar structures have been investigated based on organic,^{1–3} inorganic,^{4–6} and organic–inorganic hybrid⁷ designs and exploiting a variety of phenomena, including filament formation,^{8–10} oxygen vacancy migration,^{11–13} charge confinement,¹⁴ and redox reactions.^{1,15–18} Prominent among these examples are “resistive memories”, in which readout is the conductance of a particular region of the device.^{16–21} Resistive memories are attractive because they can be much denser and less volatile than capacitor-based DRAM and can readily be embedded in microprocessors or controllers in a wide range of applications. While many thousands of research articles have appeared on organic and inorganic resistive memories, the only variant in wide commercial use is “flash” memory based on

silicon, while “phase change” resistive memories^{22,23} have recently become commercially available.

Of particular relevance to the current report are resistive memories based on conducting polymers in which the conductance is modulated by dynamic “doping” of polythiophene^{24,25} or polypyrrole^{16,26–30} via redox reactions. We reported previously that such electrochemical doping of the polymer is reversible and repeatable many times and is correlated directly with spectroscopic monitoring of polaron formation in the polythiophene layer.³¹ Electrochemical reactions are generally avoided in organic FETs (OFETs), as they can lead to degradation via the “bias stress effect” observed upon prolonged application of bias to OFETs.^{15,32–34} The origin of “bias stress” is not completely clear, although it has been attributed to proton migration,³⁴ trapped charge,³³ and humidity affecting charge carriers.³⁵ Electrolytes incorporated into OFETs can yield much lower operating voltages in “electrolyte-gated” OFETs but also increase the risk of electrochemical reactions.^{36–39} The fundamental difference between an OFET and redox-gated memory device is that an OFET generates charge carriers (i.e., polarons) via a field effect which is present only when the source gate (SG) bias is applied,

Received: August 7, 2013

Accepted: October 14, 2013

Published: October 14, 2013

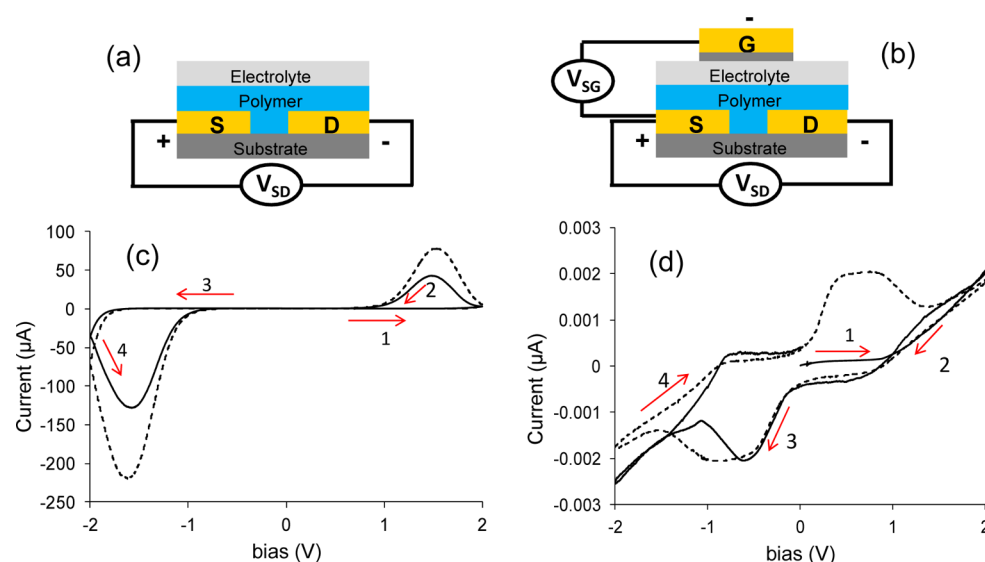


Figure 1. Schematic of the experimental devices under consideration: (a) two-terminal, open face and (b) three-terminal, top gate geometries. Electrolyte is in polyethylene oxide, as described in the text. Two-terminal (SD) I - V sweeps for (c) PQT-12 and (d) PVFc open-face devices obtained with a sweep rate of 20 mV/s. The solid lines are the first cycle, and the dotted lines are the second cycle. Note the large difference in current scale for (c) and (d).

while redox-gated resistive memory devices generate polarons electrochemically and persist after the SG bias is removed. Since both effects are possible with electrolytes present (intentional or not), it is important to understand the mechanism of a given device as well as its environmental requirements. An advantage of the redox-gated three-terminal memory devices studied in the current report is a clear relationship between the redox process and the change in resistance underlying memory action.³¹

The current research was undertaken to clarify the conditions and materials necessary for redox-gated ANVM devices based on conducting polymers and to determine the parameters affecting performance, particularly W/E speed, retention, and cycle life. We varied the polymer composition to include redox active but nonconducting poly(vinylferrocene) and also investigated electrolytes with and without an electron acceptor. The resistive switching phenomenon was fundamentally dependent on device composition, and both speed and cycle life were strongly affected by environmental changes which modulated ionic conduction. The results are valuable for designing and assessing the performance and commercial viability of redox-gated polymer memory devices.

EXPERIMENTAL SECTION

Chemicals and Materials. Polyethylene oxide (PEO, Aldrich, MW = 100 000), ethyl viologen diperchlorate (EV, 98%, Aldrich), lithium perchlorate (LiClO_4 , 99.9%, Aldrich), dimethyl sulfoxide (DMSO, 99%, Aldrich), regioregular poly(3-hexylthiophene-2,5-diyl) (P3HT, Aldrich, MW = ~ 17 500), poly(vinylferrocene) (PVFc, Polysciences Inc., MW = 50 000), polystyrene (PS, Aldrich, MW = 45 000), chlorobenzene (CB, 99%, Aldrich), toluene (anhydrous, 99.8%, Aldrich), and acetonitrile (ACN, anhydrous, 99.9%, Caledon Laboratories) were used as received. The conducting polymer, regioregular poly(3,3'-didodecylquaterthiophene) (PQT-12), was provided by Xerox Research Centre of Canada as 0.3 wt % dispersion in 1,2-dichlorobenzene.

Device Fabrication. The details of the fabrication of the memory device have been reported elsewhere.³¹ Briefly, the devices were fabricated on Si/SiO_2 (300 nm) substrates with photolithographically patterned S and D electrodes which are 0.5 mm wide with a channel

gap of 1 μm . The electrodes were prepared by e-beam evaporation of a 50 nm Au layer over a 5 nm adhesion layer of Cr. After fabrication, the devices were inspected using an optical microscope for potential defects and contaminants. The polymers were used as 0.3 wt % solutions in 1,2-dichlorobenzene (PQT and P3HT), chlorobenzene (PVFc), toluene (PS), or acetonitrile (PEO+EV) and spin-coated on clean $\text{Si}/\text{SiO}_2/\text{Au}$ substrates at 1000 rpm for 120 s to yield respective polymer films of comparable thickness (~ 25 – 35 nm). The spin-coated polymer films were annealed at 100 $^\circ\text{C}$ for 1 h, then heated to 140 $^\circ\text{C}$ at ~ 2 $^\circ\text{C}/\text{min}$ and kept at 140 $^\circ\text{C}$ for 20 min in a vacuum oven and cooled to room temperature before drop casting the electrolyte layer. The electrolyte solution was prepared by mixing equal weights of 4 wt % ethyl viologen diperchlorate [$\text{EV}(\text{ClO}_4)_2$] in acetonitrile and 5 wt % PEO in acetonitrile.³¹ The PEO solution was filtered through a 0.45 μm PTFE filter before adding the viologen solution. The electrolyte layer was deposited over the annealed polymer films by drop casting 3 μL of electrolyte solution in such a way that the electrolyte drop centers on the S–D gap. As noted in the main text, LiClO_4 was substituted for $\text{EV}(\text{ClO}_4)_2$ in a few cases, with the PEO/ LiClO_4 electrolyte prepared similarly. After drying the electrolyte layer in a house vacuum ($\sim 10^{-3}$ Torr), the devices were transferred to an electron-beam evaporator (PVD-75, Kurt J. Lesker) for the deposition of the gate electrode. The electron beam evaporator was then pumped down to a base pressure of $< 3 \times 10^{-6}$ Torr prior to the deposition of the gate electrode. The 1 mm wide gate electrodes, consisting of 15 nm carbon with 15 nm gold as the top layer, were deposited by the e-beam evaporation of respective materials through a shadow mask with an evaporation rate of 0.2–0.3 $\text{\AA}/\text{s}$ for carbon and 0.5–1.0 $\text{\AA}/\text{s}$ for Au. The gate electrode overlapped the S and D electrodes symmetrically, resulting in overlapping areas of 0.0025 cm^2 each for the S and D electrodes. The samples were stored in a nitrogen box prior to their characterization.

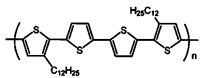
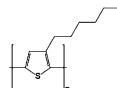
Device Characterization. The two-terminal current–voltage (I - V) measurements of the solid-state devices were performed using a Keithley 6517B electrometer or a potentiostat (CH Instruments 420 A) by connecting the working electrode lead to the S terminal and both reference and counter electrode leads at the D electrodes, as shown in Figure 1a. As noted in the figure legends, two-terminal I - V measurements were obtained similarly between the S and G electrodes in three-terminal devices. The three-terminal experiments using the configuration of Figure 1b were performed either with a Keithley 2602A dual-channel source measurement unit or National Instruments LabVIEW DAQ boards, both using in-house programs in LabVIEW or

a Keithley Test Script Builder. Although the geometry is similar to widely studied organic FETs (OFETs), the operation as an electronic device is fundamentally different. The conductance between the “S” and “D” electrodes is monitored by an applied bias, V_{SD} , while the “write” and “erase” operations are controlled by the bias applied between the source and gate, V_{SG} . Schematics for both systems are provided in the Supporting Information (SI), Figures S1 and S2. The 2602A controlled both SG and SD circuits and permitted repetitive cycling and retention tests. For example, one channel controlled the SD voltage at a fixed value while measuring the SD “readout” current, while the second channel applied an SG “write” or “erase” pulse while measuring the SG current. The LabVIEW system also controlled both channels as shown in Figure 1b but had much faster time resolution and less dynamic range. For the “dual-pulse” experiments described in Figures 4 and 5, the SD “readout” pulse occurred simultaneously with the SG “write” pulse.

RESULTS AND DISCUSSION

1. Effect of Polymer Composition. Our initial reports^{25,31} on redox-gated polythiophene ANVM used regioregular poly(3,3'-didodecylquaterthiophene) (PQT-12), developed originally for thin film transistor applications.^{40–43} To investigate the polymer properties necessary for NVM activity, PQT was compared to a more common polythiophene, P3HT, poly(vinylferrocene) (PVFc), and a redox-inactive “control” polymer, polystyrene (PS), whose structures are shown in Table 1. P3HT is widely used in organic transistors and

Table 1. Structure and Properties of Polymers Used in This Work^a

Polymer	Polymer properties		Structure
	Conducting	Redox	
PQT-12	Yes	Yes	
P3HT	Yes	Yes	
PVFc	No	Yes	
PS	No	No	

^aPQT-12 = regioregular poly(3,3'-didodecylquaterthiophene), P3HT = Poly(3-hexylthiophene-2,5-diyl) Regioregular, PVFc = Poly(vinylferrocene), PS = polystyrene.

photovoltaic devices, while PVFc is redox active but does not form conducting polarons. Figures 1c and 1d show solid-state voltammograms using the two-terminal, “open gate” geometry of Figure 1a. As shown previously,³¹ in the absence of the electrolyte layer only background currents of a few nA are observed since the polymer starts in its undoped, non-conducting state. Figure 1c shows the two-electrode voltammogram for PQT with a PEO/EV(ClO_4)₂ layer present, exhibiting conduction when the bias exceeds ~ 1.5 V for either polarity.

When the bias exceeds the “cell potential” for a PQT/EV redox reaction of ~ 1.2 V, PQT^+ is generated at the positive electrode, and EV^{+2} is reduced at the negative electrode. The observed current is presumably a combination of the Faradaic current for PQT oxidation plus direct current due to electronic conduction by the PQT^+ polarons. A similar experiment with

PVFc replacing PQT permits distinction of these two effects since PVFc does not have a conducting backbone in any oxidation state. As shown in Figure 1d, PVFc voltammetry exhibits approximately symmetric peaks at bias values of +0.8 and -0.8 V, but the peak currents are ~ 5 orders of magnitude smaller than those for PQT. Finally, omission of the electron acceptor EV from the PQT/PEO devices decreases the current by more than a factor of 10^3 since oxidation of the PQT to the conducting polaron is prevented (Supporting Information, Figure S4).

On the basis of Faraday's law, the peak areas for PVFc of $\sim 5 \times 10^{-8}$ Coulombs correspond to $\sim 2 \times 10^{-10}$ moles of electrons per cm^2 of the S or G area. In addition to this redox current, we expect some DC conduction by redox exchange, as reported for various redox polymers, including PVFc.^{44–48} The apparently ohmic behavior for $|V| > 1.5$ V is likely due to redox exchange and is discussed further below. Nevertheless, the PVFc devices clearly demonstrate that redox activity alone is not sufficient to cause the large conductance changes observed in polythiophene devices. Voltammetry for the P3HT and PS cases are shown in the Supporting Information, Figure S3, and shows negligible current for PS and behavior similar to PQT for P3HT, as expected.

Some of the artifacts and short lifetimes observed in OFETs have been attributed to residual water and its possible reactions with charge carriers and/or organic semiconductors.^{15,33–35,49,50} In the absence of EV^{+2} , water can act as a redox counter-reaction for PQT oxidation and in fact is essential for the operation of PQT/ SiO_2 ²⁵ and fluorene/ TiO_2 memory devices.^{17,18} Figure 2 shows R/W/R/E cycles for three-terminal memory devices with the structure of Figure 1b with either PEO-EV or PEO- LiClO_4 electrolytes. Although operation in vacuum significantly decreases the S–G current response for PEO-EV, the devices still show robust memory operation which may be repeated for at least hundreds of cycles. In contrast, operation of PQT/PEO- LiClO_4 devices lacking the EV electron acceptor shows negligible S–D conductance changes in vacuum. The results indicate that electrolyte alone is not sufficient for PQT oxidation, and an electron acceptor must be present. In the case of LiClO_4 in air, H_2O reduction likely accompanies PQT oxidation, and this reaction is essential for memory operation.

Figure 3 compares ten R/W/R/E memory cycles of the four different polymers in polymer/PEO-EV devices, all following overnight exposure to vacuum at $\sim 1 \times 10^{-5}$ Torr. During the memory cycles, +4 V “write” and -4 V “erase” pulses 1 s long were applied between S and G electrodes, and the SD conductivity was monitored using five readout pulses (0.5 V, 0.5 s long). PQT and P3HT show comparable switching properties of approximately equal magnitudes of conductance in the ON and OFF states.

As expected, the control devices made of polystyrene show negligible switching properties, with SD currents remaining below 1 nA for all conditions. PVFc devices show much smaller changes in SD current than PQT or P3HT, with the SD current likely due to redox exchange (see below). These results further confirm that the redox property of the polymer is not sufficient for its use as active material due to a reliance on redox hopping rather than direct electronic conduction. Furthermore, they show that the FET structure containing an electrolyte but not a conducting polymer shows an exceedingly weak memory effect.

2. Factors Affecting Memory Performance. The memory cycles displayed in Figures 2 and 3 were obtained

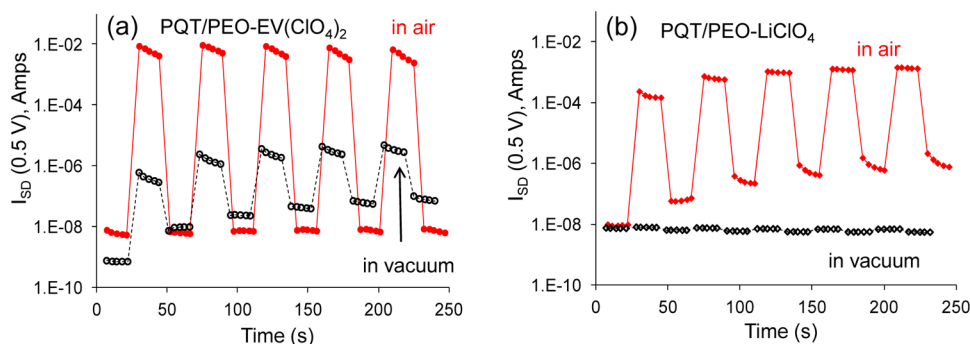


Figure 2. (a) Five W/R/E/R cycles of the PQT/PEO-EV device $V_{SG} = +3$ V “write” pulses and $V_{SG} = -3$ V “erase” pulses lasting 1 s. After each write or erase pulse, five I_{SD} values were recorded at 2 s intervals when $V_{SD} = +0.5$ V. (b) Similar response for PQT/PEO devices in which LiClO_4 was substituted for $\text{EV}(\text{ClO}_4)_2$.

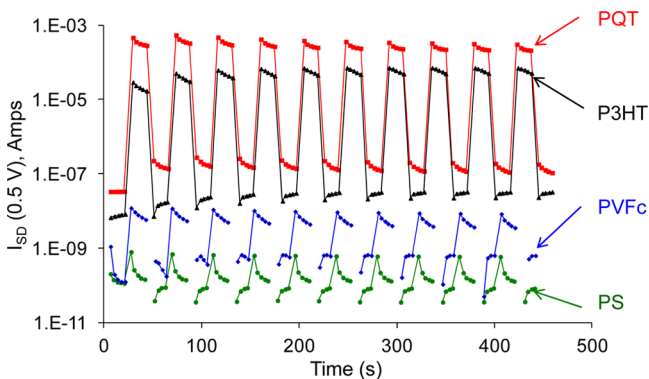


Figure 3. Ten W/R/E/R cycles using $V_{SG} = \pm 4$ V with pulse duration of 1 s for PQT, P3HT, PVFc, and PS devices. After each write or erase pulse, five I_{SD} values were recorded at 2 s intervals when $V_{SD} = +0.5$ V.

using pulses from a source measurement unit with relatively slow time resolution. To better examine the dynamics of memory operation, a “dual-pulse” experiment was developed with microsecond time resolution which could record the SG and SD currents simultaneously during and after “write” operations. Figure 4a shows the SG current response of a PQT/PEO-EV memory device during a +3 V “write” pulse between S and G electrodes commencing at $t = 0.1$ s. This procedure is essentially a chronoamperometry experiment related to the SG voltammetry shown in Figure 1c and exhibits

a charging current spike followed by a rise in current as the PQT is oxidized to its conducting form. Superimposed on the same axes is the response for PVFc/PEO-EV, showing smaller, more constant SG current after an initial charging spike. The nearly constant current for the PVFc is likely due to redox exchange across both the PVFc and EV layers between the S and G electrodes. The area under the PVFc curve corresponds to $\sim 8 \times 10^{-9}$ mol/cm², which is too large to be attributed to Faradaic current alone.

Figure 4b shows the SG response for PQT/PEO-EV superimposed with the SD response recorded simultaneously on the same device. Note the large difference in current scale, with the SD currents approximately 10^3 times larger than the SG currents, and the latency of the SD response, with the increase in current starting ~ 100 ms after the initiation of the “write” pulse. This delay has at least two likely sources: propagation of the conducting form of PQT across the channel toward the D electrode and ion transport of ClO_4^- anions in the PEO layer to compensate the space charge resulting from PQT oxidation.

The magnitudes of the redox exchange and polaron currents may be estimated from known properties of PVFc and PQT films. For conduction by PQT between the S and D electrodes yielding the ~ 1 mA ON current (at 0.5 V) corresponds to a conductivity of ~ 1.3 S/cm, well within the range reported for doped polythiophenes.^{42,43,51–54} The ~ 10 nA OFF current between S and D corresponds to a conductivity of 1.3×10^{-5}

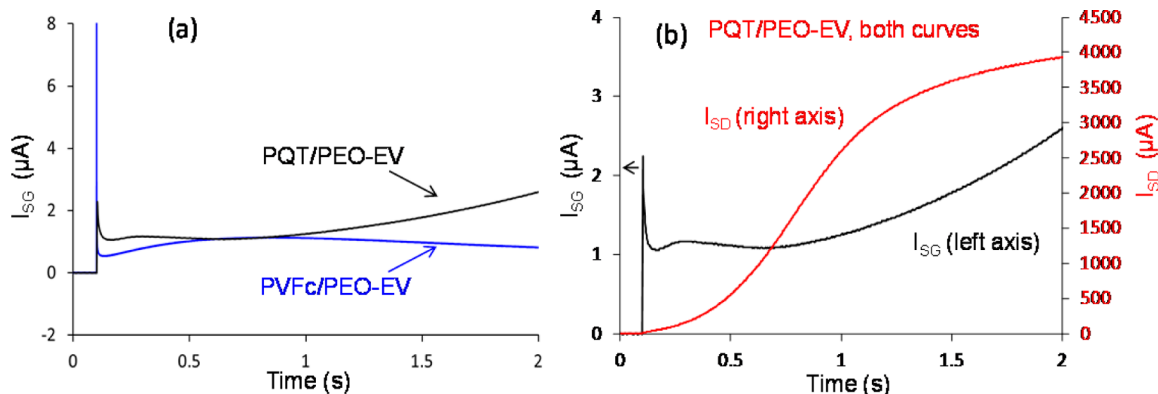


Figure 4. (a) Comparison of transient current (I_{SG}) responses for PQT/PEO-EV and PVFc/PEO-EV three-terminal devices in air. (b) Simultaneous transient current responses for the PQT/PEO-EV three-terminal device corresponding to the “write” process (I_{SG}) and “read” process (I_{SD}). The “write” voltage applied between the source and gate electrodes is $V_{SG} = +3$ V with 2 s duration, and the “read” voltage between the source and drain electrodes is $V_{SD} = +0.5$ V with same duration.

S/cm, also reasonable for undoped polythiophene. However, redox exchange currents are predicted to be much smaller, based on past work on redox polymer films. Sullivan and Murray reported electron diffusion coefficients in PVFc films of 3.2×10^{-9} cm²/s in acetonitrile vapor and $\sim 6.0 \times 10^{-10}$ in dry nitrogen.⁴⁵ Using their equations for the current resulting from redox exchange with a maximum concentration gradient of 1 M across the S–D region predicts currents of <1 nA for an electron diffusion coefficient of 6×10^{-10} cm²/s. Therefore, while redox exchange may contribute to the current across the short S–G distance, it is a negligible component of the observed S–D current for either PVFc or PQT.

Figure 5a shows the SG currents for a 0.5 s V_{SG} pulse for a single PQT/PEO-EV device, first in air, after 18 h in vacuum

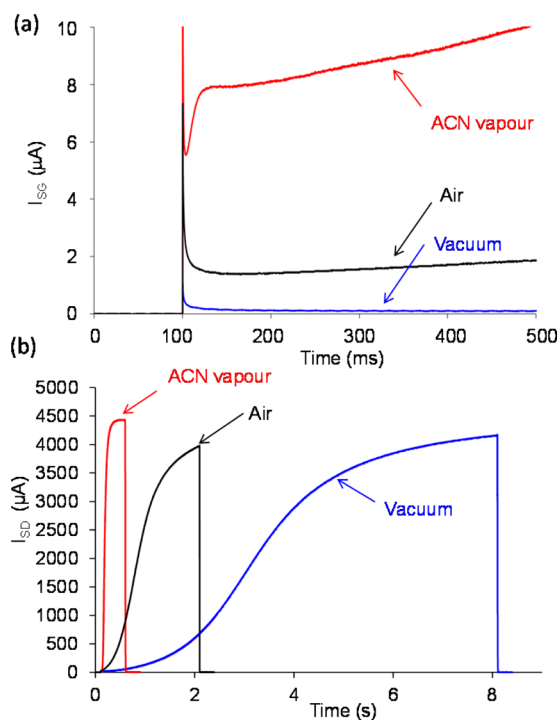


Figure 5. Transient current (I_{SG}) response of a PQT/PEO-EV(ClO_4)₂ three-terminal memory device during “write (SG)” and “read (SD)” dual-pulse measurements under different environmental conditions including air, vacuum, and ACN vapor: (a) transient current (I_{SG}) response corresponding to the “write” process and (b) simultaneous read currents monitored during “write” pulses (I_{SD}). The “write” bias between source and gate electrodes is $V_{SG} = +3$ V, and the “read” bias between source and drain electrodes is $V_{SD} = +0.5$ V. The “write” pulses in (b) were the same duration as the “read” pulses to cover the wide range of response times. Both pulses were initiated at $t = 100$ ms.

($\sim 1 \times 10^{-5}$ Torr), then after 15 min exposure to ACN vapor in the same vacuum chamber. Note that the SG currents observed in ACN vapor are approximately ten times as large as those for air and vacuum. The SD currents shown in Figure 5b show the dramatic effect of ACN vapor, with the SD response much faster in ACN compared to air. The response in vacuum is quite slow but can be accelerated using higher “write” bias, as was done for the memory cycles of Figure 3. As noted previously, the metallic gate electrode is sufficiently thin and imperfect to permit gas exchange between the atmosphere and junction interior, permitting modulation of junction performance by oxygen and water vapor.¹⁸ The exposure sequence of air, vacuum (>12 h), and ACN vapor (15 min) for the results of

Figure 5 should eliminate water as the likely cause of the acceleration observed upon ACN exposure. While ACN would only be redox active at much higher voltage, both H₂O and ACN are polar and should “solvate” ions even in a solid-state device, as reported for ion transport in solid-state redox polymers exposed to H₂O or ACN vapor.^{45,47,48} Direct evidence that ion transport determines the speed of the “write” process is provided by Figure 5a, upon closer examination of the I_{SG} currents. I_{SG} is directly proportional to the rate of generation of polarons at the S electrode and is a strong function of the local atmosphere, increasing from ~ 0.12 μA in vacuum to ~ 1.6 μA in air and ~ 9.0 μA in ACN. Therefore, polarons are generated ~ 75 times faster in ACN vapor than in a vacuum, resulting in the much faster SD response evident in Figure 5b. The nearly flat shape of the I_{SG} current during the write pulse strongly implies that resistance in the PEO-EV electrolyte is limiting the I_{SG} current, much like uncompensated resistance in a conventional electrochemical cell. There are a variety of solid-state electrolytes which have conductivities $>10^3$ higher than ClO_4^- in PEO, implying that much faster “write” times are possible through a combination of a different electrolyte and/or a thinner electrolyte layer.

As noted above, the speed of write operations may also be increased by a higher V_{SG} , consistent with polaron generation being limited by electrolyte resistance. This phenomenon may also lead to an application of redox gating to “multistate” memory, as illustrated in Figure 6. V_{SG} pulses of constant

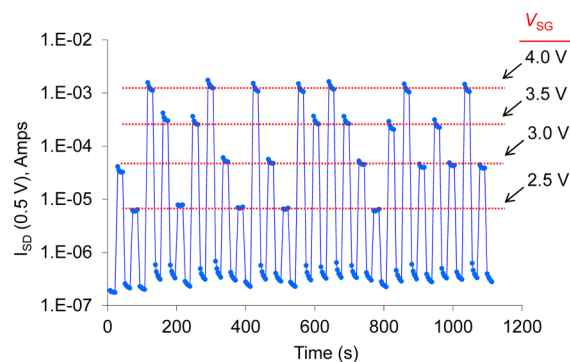


Figure 6. Multilevel W/R/E/R cycles using random $V_{SG} = \pm 2.5, 3.0, 3.5,$ and 4.0 V with pulse duration of 1 s for a PQT/PEO-EV device under vacuum ($<1 \times 10^{-5}$ Torr). After each write or erase pulse, five I_{SD} values were recorded at 2 s intervals when $V_{SD} = +0.5$ V.

duration (1 s) but varying magnitude generate distinguishable and reproducible SD conductance values with a range of ON/OFF conductance from ~ 10 to $>10^3$. These states may be generated and interrogated randomly by variations in “write” voltage. At least in principle, the number of bits available in one memory cell could be increased by a factor of 4 using this approach.

We reported previously that PQT/PEO-EV devices could be cycled through complete R/W/R/E sequences at least 200 times in vacuum with only minor changes in the “ON” and “OFF” currents.³¹ After 2000 cycles in vacuum, the ON current shown in Supporting Information, Figure S6, decreases from 7 mA to 3 μA , but the ON/OFF current ratio remains above 100. The decrease is more rapid when devices were cycled in air, although the ON/OFF ratio remains above 10 after 1000 cycles (see Supporting Information, Figure S5). Prolonged exposure of “resting” devices to O₂ and H₂O for months in air had little

effect on performance, indicating that degradation was observed only during W/E cycling. Endurance was tested during cycling in various atmospheres, with the “read” currents following each W and E pulse shown in Figure 7. For each colored trace, a

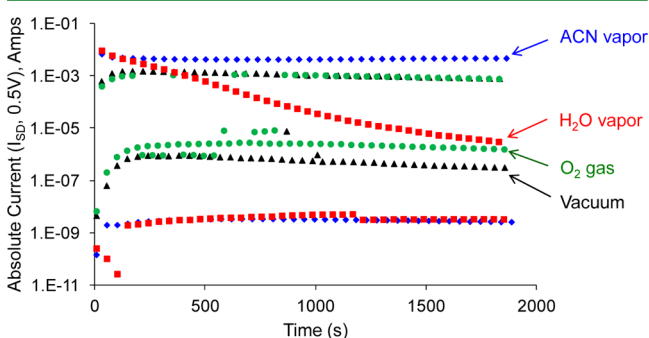


Figure 7. Comparison of 40 W/R/E/R memory cycles of PQT/PEO-EV devices in vacuum, O₂ gas, ACN, and H₂O vapor. The data represent the variation of SD “readout” currents after 4 V SG “write” or “erase” pulses of 2 s duration. Absolute values of current shown due to transient negative currents of ~ 1 nA for the ACN and H₂O cases.

fresh device was first exposed to vacuum ($\sim 1 \times 10^{-5}$ Torr) for five hours, and then the chamber was backfilled with gaseous H₂O, ACN, or O₂. Endurance in O₂ was comparable to that in vacuum, although the OFF current was higher, presumably due to slight PQT oxidation by the atmosphere.⁵¹ H₂O vapor significantly accelerated degradation but also decreased the OFF current to negligible values compared to those in vacuum. ACN vapor not only increased the ON/OFF ratio to the highest yet observed ($>10^6$) but also decreased the degradation rate.

Note that both water and ACN vapor increase the ON/OFF ratio, consistent with the proposal that polar molecules both increase ion mobility and reduce uncompensated resistance. Irreversible degradation of the devices observed in air or water vapor is likely due to “overoxidation” of the PQT with possible sulfoxide formation, which has been reported for polythiophenes in acetonitrile and thin film transistors.^{30,35,49,50}

The redox reactions and ion transport which underlie memory operation for three-terminal redox-gated polymer memory devices are shown in Figure 8 for PVFc/PEO-EV (upper panels) and PQT/PEO-EV (lower panels). Both polymers are initially in their neutral states, with very low conductance between S and D electrodes. Upon application of a positive V_{SG} “write” pulse, both polymers are oxidized at the S electrode, countered by reduction of EV⁺² at the G electrode. For PVFc, the rate of redox hopping is small enough to generate a small S–G current and an even smaller S–D current across the much larger distance between the S and D electrode. For PQT, the oxidized polaron is a conductor, which can propagate across the gap as a “moving electrode” to bring about oxidation of the entire region between S and D, thus permitting a large SD current in the ON state. The increase of the SD current lags the SG current due to the time required for propagation of the conducting phase across the SD gap and the finite rate of anion motion in the electrolyte and PQT layers. Finally, the reader is reminded that the polymer NVM devices investigated here differ fundamentally from “electrolyte-gated” organic field-effect transistors (OFETs), in that redox reactions are intentional in memory devices to form polarons and provide bistability, while the OFETs rely on electrostatic

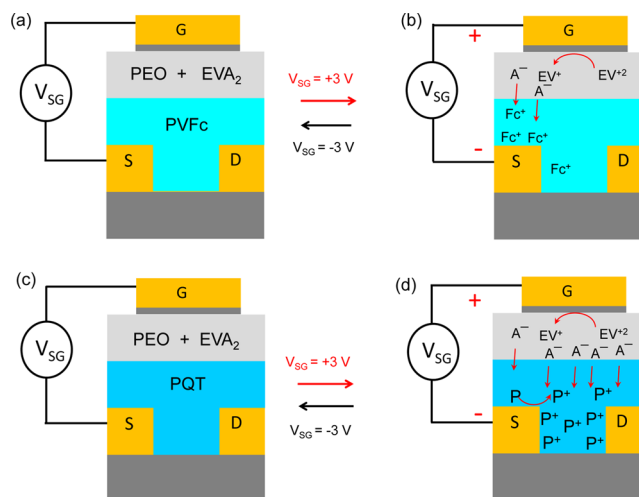


Figure 8. Schematic drawings of mechanisms for the PVFc/PEO-EV (a, b) and PQT/PEO-EV (c, d) memory devices. The positive V_{SG} pulse oxidizes the polymer and reduced EV⁺² to EV⁺, accompanied by transport of ClO₄[−] (A[−]) from PEO to the oxidized polymer.

doping which is only present during application of a gate bias.^{36–39}

CONCLUSIONS

In summary, the results showing the effect of composition and atmosphere on redox-gated three-terminal polymer memory devices reveal several important points about the memory mechanism and performance. First, the active polymer layer must change conductivity during a redox event, and redox activity alone is not sufficient for a significant memory effect. Second, an electron acceptor must be present to permit generation of conducting polarons, and both water and ethyl viologen can act as the acceptor. However, devices lacking EV are sensitive to atmosphere and less stable than those containing EV due to degradative reactions between polarons and H₂O. Third, the transition between the conducting and nonconducting states during W/E cycles is limited by the rate of ion motion within the electrolyte layer, and this rate is much higher when polar acetonitrile vapor is present. Available solid-state electrolytes should enable increases in W/E speed of several orders of magnitude. Furthermore, changes in device geometry and electrolyte layer thickness guided by the constraints of electrolyte conductivity should also allow significant speed improvements, possibly into the submilli-second range or faster. Fourth, electrolyte resistance may be partially overcome by increasing the V_{SG} voltage, leading to the possibility of redox-gated multistate memory having five distinguishable conductance states for V_{SG} ranging from 2.5 to 4.0 V. Fifth, device endurance is extended significantly as residual H₂O is replaced by acetonitrile, and atmospheric oxygen has little effect on device stability. The improved understanding of the memory mechanism and requirements resulting from the current results provide a “road map” for improvements in speed, retention, and cycle life. We are currently modifying cell design and conducting a detailed analysis of the switching dynamics, with close attention to performance relative to other alternative NVM devices. The redox-gated polymer memory devices described here may have significant advantages over existing “flash” memory due to their

lower W/E voltage requirements, extended cycle life, and the possibility of multistate operation in a single cell.

■ ASSOCIATED CONTENT

■ Supporting Information

Schematics for Keithley 2602 SMU and LabVIEW interfaces, two terminal I – V response for P3HT and PS devices, two terminal I – V responses for PQT with various electrolytes, 1000 R/W/R/E memory cycles of three-terminal memory devices in air and vacuum, 2000 R/W/R/E cycles of three-terminal memory. This material is available free of charge via the Internet at <http://pubs.acs.org>.

■ AUTHOR INFORMATION

Corresponding Author

*E-mail: mccreery@ualberta.ca.

Author Contributions

[†]These authors contributed equally to the research.

Notes

The authors declare no competing financial interest.

■ ACKNOWLEDGMENTS

The authors acknowledge financial support from the National Institute for Nanotechnology, the Natural Sciences and Engineering Research Council of Canada, Alberta Nanoworks, and the Xerox Research Centre of Canada (XRCC). The authors thank Nikola Pekas for useful conversations and Bryan Szeto for developing the LabVIEW dual pulse experiment.

■ REFERENCES

- (1) Heremans, P.; Gelinck, G. H.; Müller, R.; Baeg, K.-J.; Kim, D.-Y.; Noh, Y.-Y. *Chem. Mater.* **2011**, *23*, 341–358.
- (2) Ling, Q.-D.; Liaw, D.-J.; Zhu, C.; Chan, D. S.-H.; Kang, E.-T.; Neoh, K.-G. *Prog. Polym. Sci.* **2008**, *33*, 917–978.
- (3) Scott, J. C.; Bozano, L. D. *Adv. Mater.* **2007**, *19*, 1452–1463.
- (4) Waser, R.; Aono, M. *Nat. Mater.* **2007**, *6*, 833–840.
- (5) Waser, R.; Dittmann, R.; Staikov, G.; Szot, K. *Adv. Mater.* **2009**, *21*, 2632–2663.
- (6) Das, B. C.; Pal, A. J. *Small* **2008**, *4*, 542–547.
- (7) Das, B. C.; Pal, A. J. *ACS Nano* **2008**, *2*, 1930–1938.
- (8) Kozicki, M. N.; Park, M.; Mitkova, M. *IEEE Trans. Nanotechnol.* **2005**, *4*, 331–338.
- (9) Mitkova, M.; Kozicki, M. N.; Kim, H. C.; Alford, T. L. *Thin Solid Films* **2004**, *449*, 248–253.
- (10) Ouyang, J.; Chu, C.-W.; Szmanda, C. R.; Ma, L.; Yang, Y. *Nat. Mater.* **2004**, *3*, 918–922.
- (11) Strukov, D. B.; Williams, R. S. *Appl. Phys. A: Mater. Sci. Process.* **2009**, *94*, 515–519.
- (12) Strukov, D. B.; Snider, G. S.; Stewart, D. R.; Williams, R. S. *Nature* **2008**, *453*, 80–83.
- (13) Agapito, L. A.; Alkis, S.; Krause, J. L.; Cheng, H.-P. *J. Phys. Chem. C* **2009**, *113*, 20713–20718.
- (14) Verbakel, F.; Meskers, S. C. J.; Janssen, R. A. J. *Appl. Phys. Lett.* **2006**, *89*, 102103.
- (15) Baeg, K.-J.; Noh, Y.-Y.; Ghim, J.; Lim, B.; Kim, D.-Y. *Adv. Funct. Mater.* **2008**, *18*, 3678–3685.
- (16) Hong, J.-Y.; Jeon, S. O.; Jang, J.; Song, K.; Kim, S. H. *Org. Electron.* **2013**, *14*, 979–983.
- (17) Wu, J.; Mobley, K.; McCreery, R. J. *Chem. Phys.* **2007**, *126*, 24704.
- (18) Wu, J.; McCreery, R. L. *J. Electrochem. Soc.* **2009**, *156*, P29–P37.
- (19) Akihito, S. *Mater. Today* **2008**, *11*, 28–36.
- (20) Yang, J. J.; Pickett, M. D.; Li, X.; Ohlberg, D. A. A.; Stewart, D. R.; Williams, R. S. *Nat. Nanotechnol.* **2008**, *3*, 429–433.
- (21) Linn, E.; Rosezin, R.; Kugeler, C.; Waser, R. *Nat. Mater.* **2010**, *9*, 403–406.
- (22) Caldwell, M. A.; Jeyasingh, R. G. D.; Wong, H. S. P.; Milliron, D. J. *Nanoscale* **2012**, *4*, 4382–4392.
- (23) Nardone, M.; Simon, M.; Karpov, I. V.; Karpov, V. G. *J. Appl. Phys.* **2012**, *112*, 071101–071120.
- (24) Ghosh, B.; Pal, A. J. *J. Phys. Chem. C* **2009**, *113*, 18391–18395.
- (25) Shoute, L.; Pekas, N.; Wu, Y.; McCreery, R. *Appl. Phys. A: Mater. Sci. Process.* **2011**, *102*, 841–850.
- (26) Barman, S.; Deng, F.; McCreery, R. L. *J. Am. Chem. Soc.* **2008**, *130*, 11073–11081.
- (27) Rahman, G. M. A.; Zhao, J.-H.; Thomson, D. J.; Freund, M. S. *J. Am. Chem. Soc.* **2009**, *131*, 15600–15601.
- (28) Zhao, J. H.; Thomson, D. J.; Pillai, R. G.; Freund, M. S. *Appl. Phys. Lett.* **2009**, *94*, 092113.
- (29) Pillai, R. G.; Zhao, J. H.; Freund, M. S.; Thomson, D. J. *Adv. Mater.* **2008**, *20*, 49–53.
- (30) Shin, K.-H.; Cho, J.; Jang, J.; Jang, H. S.; Park, E. S.; Song, K.; Kim, S. H. *Org. Electron.* **2012**, *13*, 715–720.
- (31) Kumar, R.; Pillai, R. G.; Pekas, N.; Wu, Y.; McCreery, R. L. *J. Am. Chem. Soc.* **2012**, *134*, 14869–14876.
- (32) Bobbert, P. A.; Sharma, A.; Mathijssen, S. G. J.; Kemerink, M.; de Leeuw, D. M. *Adv. Mater.* **2012**, *24*, 1146–1158.
- (33) Mathijssen, S. G. J.; Spijkman, M.-J.; Andringa, A.-M.; van Hal, P. A.; McCulloch, I.; Kemerink, M.; Janssen, R. A. J.; de Leeuw, D. M. *Adv. Mater.* **2010**, *22*, 5105–5109.
- (34) Sharma, A.; Mathijssen, S. G. J.; Kemerink, M.; de Leeuw, D. M.; Bobbert, P. A. *Appl. Phys. Lett.* **2009**, *95*, 253305–253303.
- (35) Chabinyk, M. L.; Endicott, F.; Vogt, B. D.; DeLongchamp, D. M.; Lin, E. K.; Wu, Y.; Liu, P.; Ong, B. S. *Appl. Phys. Lett.* **2006**, *88*, 113514–113513.
- (36) Lee, J.; Kaake, L. G.; Cho, J. H.; Zhu, X.-Y.; Lodge, T. P.; Frisbie, C. D. *J. Phys. Chem. C* **2009**, *113*, 8972–8981.
- (37) Panzer, M. A.; Frisbie, C. D. *Adv. Funct. Mater.* **2006**, *16*, 1051–1056.
- (38) Panzer, M. J.; Frisbie, C. D. *J. Am. Chem. Soc.* **2007**, *129*, 6599–6607.
- (39) Panzer, M. J.; Frisbie, C. D. *J. Am. Chem. Soc.* **2005**, *127*, 6960–6961.
- (40) Liu, P.; Wu, Y.; Pan, H.; Li, Y.; Gardner, S.; Ong, B. S.; Zhu, S. *Chem. Mater.* **2009**, *21*, 2727–2732.
- (41) Wu, Y.; Liu, P.; Gardner, S.; Ong, B. S. *Chem. Mater.* **2004**, *17*, 221–223.
- (42) Ong, B. S.; Wu, Y.; Liu, P.; Gardner, S. *J. Am. Chem. Soc.* **2004**, *126*, 3378–3379.
- (43) Ong, B. S.; Wu, Y.; Liu, P.; Gardner, S. *Adv. Mater.* **2005**, *17*, 1141–1144.
- (44) Daum, P.; Lenhard, J. R.; Rolison, D.; Murray, R. W. *J. Am. Chem. Soc.* **1980**, *102*, 4649–4653.
- (45) Sullivan, M. G.; Murray, R. W. *J. Phys. Chem.* **1994**, *98*, 4343–4351.
- (46) Terrill, R. H.; Hatazawa, T.; Murray, R. W. *J. Phys. Chem.* **1995**, *99*, 16676–16683.
- (47) Terrill, R. H.; Murray, R. W. In *Molecular Electronics*; Jortner, J., Ratner, M., Eds.; Blackwell Science Ltd.: Oxford, U.K., 1997; pp 215–239.
- (48) Terrill, R. H.; Sheehan, P. E.; Long, V. C.; Washburn, S.; Murray, R. W. *J. Phys. Chem.* **1994**, *98*, 5127–5134.
- (49) Barsch, U.; Beck, F. *Electrochim. Acta* **1996**, *41*, 1761–1771.
- (50) Kaihovirta, N.; Aarnio, H.; Wikman, C.-J.; Wilén, C.-E.; Österbacka, R. *Adv. Funct. Mater.* **2010**, *20*, 2605–2610.
- (51) Liu, C.-C.; Yang, C.-M.; Liu, W.-H.; Liao, H.-H.; Horng, S.-F.; Meng, H.-F. *Synth. Met.* **2009**, *159*, 1131–1134.
- (52) Masuda, H.; Asano, D. K.; Kaeriyama, K. *Synth. Met.* **1997**, *84*, 209–210.
- (53) Johansson, E.; Larsson, S. *Synth. Met.* **2004**, *144*, 183–191.
- (54) Ofer, D.; Crooks, R. M.; Wrighton, M. S. *J. Am. Chem. Soc.* **1990**, *112*, 7869–7879.